

Off-Line Programmed Error Compensation of an Industrial Robot in Ship Hull Welding

Guanglei Wu^(✉), Delun Wang, and Huimin Dong

School of Mechanical Engineering, Dalian University of Technology,
Dalian 116024, China
{gwu, dlunwang, donghm}@dlut.edu.cn

Abstract. This paper presents the compliance modeling and error compensation for an industrial robot in the application of ship hull welding. The Cartesian stiffness matrix is derived using the virtual-spring approach, which takes the actuation and structural stiffness, arm gravity and external loads into account. Based on the developed stiffness model, a method to compensate the compliance error is introduced, being illustrated with an industrial robot along a welding trajectory. The results show that this compensation method can effectively improve the robot's operational accuracy, allowing the actual trajectory of the robot with auxiliary loads to coincide with the target one approximately.

Keywords: Industrial robot · Hull welding · Kinetostatics · Gravity effect · Error compensation

1 Introduction

As an automatic manufacturing device, industrial robots have been widely used and play an important role in many fields of industrial applications, thanks to their high repeatability accuracy and operational stability. Amongst the industrial applications, this type of serial manipulators are well adapted in welding industry [3], such as auto industry. Besides, the robots can also be used in ship-building industry, i.e., the large-scale hull welding, as displayed in Fig. 1. In this procedure, the welding trajectory is firstly detected by the vision system, where the data of the trajectory will be transferred to the control system for robot programming to accomplish the welding procedure. This means that the robot will conduct an off-line task.

The robots' motions are usually generated via the robotic controllers by virtue of the inverse kinematic model to compute the input signals for actuators corresponding to the desired end-effector position, where the compliance errors are ignored. On the other hand, as depicted in Fig. 1(c), under certain external load, particularly, the arm gravity and dynamic inertial forces, the kinematic control becomes non-applicable due to the elastic compliance errors caused by the limited strength of the robot components [12], namely, the actual trajectory

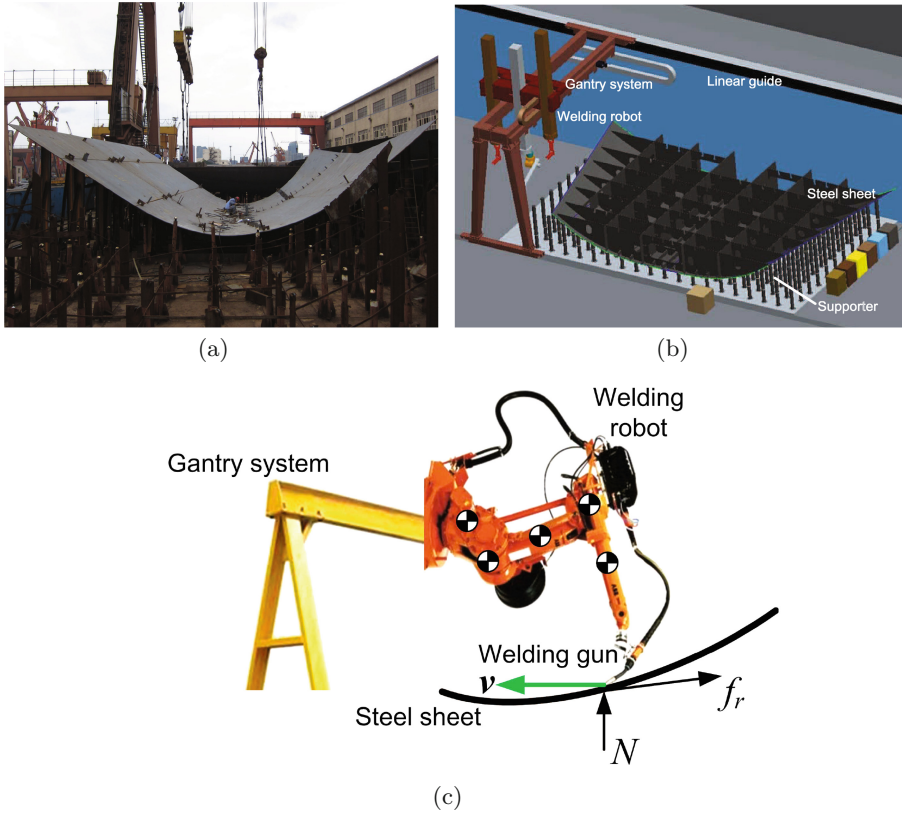


Fig. 1. The robot-based ship hull welding: (a) steel sheet on the supporter; (b) overall scheme; (c) reaction forces onto the welding gun.

will shift away from the desired path, resulting in the decreased product quality wherefrom high precision is needed in the applications.

The compliance error, i.e., geometric changes of the robot end-effector, can be compensated through the calibration [7, 21], whereas, this technique is sometimes expensive. An economic way to handle the problem of error compensation is the modification of the robot control scheme [6, 10] that defines the prescribed trajectory in Cartesian space: based on the error model, the loaded input trajectory is regenerated to achieve the coincidence between the output trajectory and the desired one, while input trajectory differs from the target one. The modification of the input trajectory is to be based on the compliance error model that calls for the computation of the stiffness matrix [8]. The stiffness matrix for the serial robotics was first derived by Salisbury [15], where only the actuation compliance described by one-dimensional linear springs was considered. In this approach, the derivation of the stiffness is on the basis of the assumption that the manipulator is in an unloaded equilibrium configuration. In practice, the

external loads directly influence on the manipulator equilibrium configuration and may modify the stiffness properties [2,4]. As a consequence, the structural compliance and the robot geometry change due to external loads and gravity should be considered [11,13,14]. Thus, this work focuses on the compliance error modeling and compensation that is able to take into account the influence of the external and internal wrenches and robot gravity onto the stiffness matrix and elastic deformations.

This paper deals with the stiffness modeling and compliance error compensation of an industrial robot in ship hull welding. The Cartesian stiffness matrix is computed in loaded configurations, where the actuation and structural stiffness is considered as well as the influence of the arm gravity and external loads. A method to modify the input trajectory is presented for error compensation. This method is numerically illustrated with the welding robot along a trajectory and the results show the effectiveness of the error compensation approach.

2 Industrial Welding Robot

Figure 2 shows the ABB IRB4600.60/205 robot [1] as the welding robot in this project. IRB 4600 series is ABB Robotics pioneer of the new sharp generation with enhanced and new capabilities, of which one industrial application is dedicated to welding.

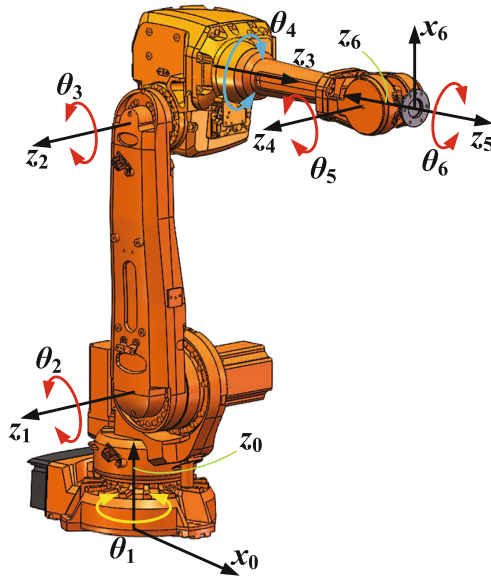


Fig. 2. The ABB IRB4600.60/205 robot and its coordinate systems.

2.1 Kinematics of the Industrial Robot

Following the Denavit–Hartenberg (D–H) convention [5], the Cartesian coordinate systems are established for each link of the robotic arm as shown in Fig. 2. Hereafter, let \mathbf{i} , \mathbf{j} and \mathbf{k} be the unit vectors along x -, y - and z -axis, respectively. The transformation matrix in the forward kinematics of the end-effector in the reference frame (x_0, y_0, z_0) is expressed as

$${}^0\mathbf{A}_6 = \begin{bmatrix} \mathbf{R} & \mathbf{q} \\ \mathbf{0} & 1 \end{bmatrix} = \prod_{i=1}^6 {}^{i-1}\mathbf{A}_i \quad \text{where} \quad {}^{i-1}\mathbf{A}_i = \begin{bmatrix} {}^{i-1}\mathbf{R}_i & {}^{i-1}\mathbf{q}_i \\ \mathbf{0} & 1 \end{bmatrix} \quad (1)$$

with

$${}^{i-1}\mathbf{R}_i = \mathbf{R}_{z_{i-1}}(\theta_i)\mathbf{R}_{x_i}(\alpha_i) \quad (2a)$$

$${}^{i-1}\mathbf{q}_i = [a_i \cos \alpha_i \ a_i \sin \alpha_i \ d_i]^T \quad (2b)$$

where the D–H parameters are listed in Table 1. The inverse geometry problem of the six-axis robotics has been well documented in the literature [16].

Table 1. D-H parameters of the IRB4600_60/205 robot.

Joint i	α_i	a_i [m]	d_i [m]	θ_i
1	$\pi/2$	0.175	0.495	θ_1
2	0	1.075	0	θ_2
3	$\pi/2$	0.175	0	θ_3
4	$-\pi/2$	0	0.960	θ_4
5	$\pi/2$	0	0	θ_5
6	π	0	0.135	θ_6

2.2 Jacobian Matrix

The joint angular velocity can be calculated with the Jacobian matrix as below:

$$\dot{\boldsymbol{\theta}} = \mathbf{J}^{-1}\dot{\mathbf{t}} \quad (3)$$

where $\dot{\boldsymbol{\theta}} = [\dot{\theta}_1 \ \dot{\theta}_2 \ \dots \ \dot{\theta}_6]^T$ denotes the vector of the joint angular velocities, and $\dot{\mathbf{t}} = [\boldsymbol{\omega}^T \ \dot{\mathbf{q}}^T]^T$ stands for the end-effector twist, $\boldsymbol{\omega}$ being the angular velocities. Moreover, \mathbf{J} is the Jacobian matrix of the robotic arm [17], namely,

$$\mathbf{J} = [\mathbf{j}_1 \ \mathbf{j}_2 \ \dots \ \mathbf{j}_6] \quad \text{where} \quad \mathbf{j}_i = \begin{bmatrix} \mathbf{z}_{i-1} \\ \mathbf{p}_{i-1} \times \mathbf{z}_{i-1} \end{bmatrix} \quad (4)$$

with

$$\mathbf{z}_{i-1} = \mathbf{R}_{i-1}\mathbf{k}; \quad \mathbf{p}_{i-1} = \mathbf{q}_{i-1} - \mathbf{q} \quad (5)$$

where \mathbf{R}_{i-1} and \mathbf{q}_{i-1} denote the rotation matrix and position vector of the transformation matrix from the reference coordinate system to the $(i-1)$ th coordinate system, respectively, which can be extracted from $\prod_{i=0}^{i-1} {}^{i-1}\mathbf{A}_i$ in Eq. (1).

2.3 Robot Dynamics

The dynamic behavior of the robot under the load \mathbf{f}_e during the welding can be described as

$$\mathbf{M}\delta\ddot{\mathbf{t}} + \mathbf{C}\delta\dot{\mathbf{t}} + \mathbf{K}\delta\mathbf{t} = \mathbf{f}_e \quad (6)$$

where \mathbf{M} is 6-dimensional mass matrix that represents the global behavior of the robot in terms of natural frequencies, \mathbf{C} is 6-dimensional damping matrix, and \mathbf{K} is 6-dimensional Cartesian stiffness matrix of the robot under the external loading \mathbf{f}_e [18]. Moreover, $\delta\mathbf{t}$, $\delta\dot{\mathbf{t}}$ and $\delta\ddot{\mathbf{t}}$ are the instantaneous dynamic displacement, velocity and acceleration of the tool end-point, respectively.

The mass matrix \mathbf{M} in Eq. (6) can be solved based on the dynamic equation of motion (EOM) [9] of a serial robot as below:

$$\mathbf{M}(\boldsymbol{\theta})\ddot{\boldsymbol{\theta}} + \mathbf{v}(\boldsymbol{\theta}, \dot{\boldsymbol{\theta}}) + \mathbf{g}(\boldsymbol{\theta}) = \boldsymbol{\tau} \quad (7)$$

where $\boldsymbol{\theta}$, $\dot{\boldsymbol{\theta}}$, $\ddot{\boldsymbol{\theta}}$ are 6-dimensional vectors of generalized joint angles, angular velocities, and angular accelerations, respectively. $\mathbf{M}(\boldsymbol{\theta})$ is the 6×6 general inertial matrix, $\mathbf{v}(\boldsymbol{\theta}, \dot{\boldsymbol{\theta}})$ is a 6-dimensional vector representing the Coriolis and centrifugal forces, and $\mathbf{g}(\boldsymbol{\theta})$ is a 6-dimensional vectors accounting for the force due to gravity. Moreover, $\boldsymbol{\tau}$ is the vector of general external forces applied at joints.

3 Compliance Error Modeling and Compensation

In order to compensate the positioning errors of the robot end-effector for high-quality welding, the compliance errors caused by the external payloads and robot gravity should be calculated precisely, which calls for the computation of the stiffness matrix of the robot.

3.1 Elastostatic Modeling

In this work, the virtual spring approach [13] is adopted to derive the stiffness matrix, based on the screw coordinates [19,20]. Figure 3 shows the VJM model of the robotic arm, where \mathbf{g}_j , $j = 1, 2, \dots, 8$, stand for the gravity and \mathbf{f}_e denotes the external loads.

Let $\boldsymbol{\theta}$, $\boldsymbol{\theta}'$ be the original and the deformed angular displacements of the joints, respectively, in accordance with the principle of virtual work, the work of the auxiliary loads is equal to the work of internal forces $\boldsymbol{\tau}_\theta$ [13], namely,

$$\sum (\mathbf{g}_j^T \delta\mathbf{t}_j) + \mathbf{f}_e^T \delta\mathbf{t} = \boldsymbol{\tau}_\theta^T (\boldsymbol{\theta}' - \boldsymbol{\theta}) \quad (8)$$

where the virtual displacements $\delta\mathbf{t}_j$ and $\delta\mathbf{t}$ can be computed from the linearized geometrical model derived from $\delta\mathbf{t}_j = \mathbf{J}_j(\boldsymbol{\theta}' - \boldsymbol{\theta})$ and $\delta\mathbf{t} = \mathbf{J}_\theta(\boldsymbol{\theta}' - \boldsymbol{\theta})$, respectively, \mathbf{J}_j and \mathbf{J}_θ being the Jacobians, namely,

$$\mathbf{J}_\theta = [\mathbf{j}_1 \ \mathbf{j}_2 \ \mathbf{J}_U \ \mathbf{j}_3 \ \mathbf{j}_4 \ \mathbf{J}_F \ \mathbf{j}_5 \ \mathbf{j}_6] \in \mathbb{R}^{6 \times 18} \quad (9)$$

$$\mathbf{J}_j = \mathbf{J}_\theta(:, 1:k) \quad (10)$$

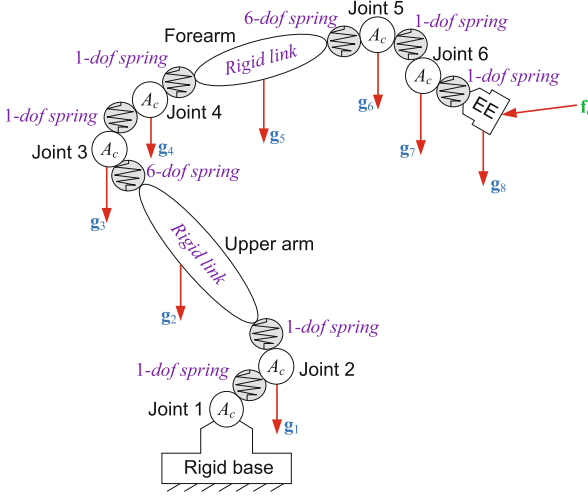


Fig. 3. Virtual-spring model of the industrial robot with auxiliary loads, where A_c and EE stand for the actuator and end-effector, respectively.

where $\mathbf{J}_\theta(:, 1:k)$ stands for the first k columns in \mathbf{J}_θ and k stands for the number of the mobilities of the virtual springs from the base to \mathbf{g}_j . Moreover, \mathbf{J}_U and \mathbf{J}_F , respectively, relate the link deflections of the upper arm and forearm to the end-effector, expressed as

$$\mathbf{J}_U = \begin{bmatrix} \mathbf{x}_1 & \mathbf{y}_1 & \mathbf{z}_1 & \mathbf{0} & \mathbf{0} & \mathbf{0} \\ \mathbf{q}_2 \times \mathbf{x}_1 & \mathbf{q}_2 \times \mathbf{y}_1 & \mathbf{q}_2 \times \mathbf{z}_1 & \mathbf{x}_1 & \mathbf{y}_1 & \mathbf{z}_1 \end{bmatrix} \quad (11a)$$

$$\mathbf{J}_F = \begin{bmatrix} \mathbf{z}_3 & \mathbf{x}_3 & \mathbf{y}_3 & \mathbf{0} & \mathbf{0} & \mathbf{0} \\ \mathbf{q}_4 \times \mathbf{z}_3 & \mathbf{q}_4 \times \mathbf{x}_3 & \mathbf{q}_4 \times \mathbf{y}_3 & \mathbf{z}_3 & \mathbf{x}_3 & \mathbf{y}_3 \end{bmatrix} \quad (11b)$$

Equation (8) is rewritten as

$$\sum (\mathbf{g}_j^T \mathbf{J}_j (\boldsymbol{\theta}' - \boldsymbol{\theta})) + \mathbf{f}_e^T \mathbf{J}_\theta (\boldsymbol{\theta}' - \boldsymbol{\theta}) = \boldsymbol{\tau}_\theta^T (\boldsymbol{\theta}' - \boldsymbol{\theta}) \quad (12)$$

sequentially, the force equilibrium equation for the robotic arm is derived as

$$\boldsymbol{\tau}_\theta = \sum (\mathbf{J}_j^T \mathbf{g}_j) + \mathbf{J}_\theta^T \mathbf{f}_e = \mathbf{J}_g^T \mathbf{G} + \mathbf{J}_\theta^T \mathbf{F} \quad (13)$$

with

$$\mathbf{J}_g^T = [\mathbf{J}_1 \ \mathbf{J}_2 \ \dots \ \mathbf{J}_8] \in \mathbb{R}^{6 \times 48}; \quad \mathbf{G} = [\mathbf{g}_1^T \ \mathbf{g}_2^T \ \dots \ \mathbf{g}_8^T]^T \in \mathbb{R}^{48} \quad (14)$$

With the linear force-deflection relation, the equilibrium condition is written as

$$\mathbf{J}_\theta^T \mathbf{G} + \mathbf{J}_\theta^T \mathbf{f}_e = \mathbf{K}_\theta (\boldsymbol{\theta}'_i - \boldsymbol{\theta}_i) \quad (15)$$

with the stiffness matrix \mathbf{K}_θ in the joint space expressed as

$$\mathbf{K}_\theta = \text{diag} [K_{\text{act},1} \ K_{\text{act},2} \ \mathbf{K}_U \ K_{\text{act},3} \ K_{\text{act},4} \ \mathbf{K}_F \ K_{\text{act},5} \ K_{\text{act},6}] \quad (16)$$

where $K_{\text{act},i}$ is the actuation stiffness, and \mathbf{K}_U and \mathbf{K}_F , calculated by the Euler-Bernoulli beam model, represent the 6×6 stiffness matrices of the upper arm and forearm, respectively.

To compute the stiffness matrix of the loaded mode, let assume that a neighborhood of the loaded configuration, where the external loads and the joint displacement are supposed to be incremented by some small values $\delta \mathbf{f}_e$ and $\delta \boldsymbol{\theta}$, also satisfies the equilibrium conditions, leading to

$$(\mathbf{J}_g + \delta \mathbf{J}_g)^T \mathbf{G} + (\mathbf{J}_\theta + \delta \mathbf{J}_\theta)^T (\mathbf{f}_e + \delta \mathbf{f}_e) = \mathbf{K}_\theta (\boldsymbol{\theta}' - \boldsymbol{\theta} + \delta \boldsymbol{\theta}) \quad (17)$$

with the linearized kinematic constraint:

$$\delta \mathbf{t} = \mathbf{J}_\theta \delta \boldsymbol{\theta} \quad (18)$$

Upon the removal of the unchanged equilibrium condition of Eq. (15) from Eq. (17), after linearization, one obtains

$$\mathbf{H}_g^T \otimes \mathbf{G} \delta \boldsymbol{\theta} + \mathbf{J}_\theta^T \delta \mathbf{f}_e + \mathbf{H}_\theta^T \otimes \mathbf{f}_e \delta \boldsymbol{\theta} = \mathbf{K}_\theta \delta \boldsymbol{\theta} \quad (19)$$

where the symbol \otimes represents the Kronecker product between matrices, and $\mathbf{H}_g = \partial \mathbf{J}_g / \partial \boldsymbol{\theta}$, $\mathbf{H}_\theta = \partial \mathbf{J}_\theta / \partial \boldsymbol{\theta}$, namely, the Hessian matrices. Combing Eqs. (18) and (19), the kineto-static model of the industrial robot is reduced to

$$\begin{bmatrix} \mathbf{0} & \mathbf{J}_\theta \\ \mathbf{J}_\theta^T & \mathbf{K}_E - \mathbf{K}_\theta \end{bmatrix} \begin{bmatrix} \delta \mathbf{f}_e \\ \delta \boldsymbol{\theta} \end{bmatrix} = \begin{bmatrix} \delta \mathbf{t} \\ \mathbf{0} \end{bmatrix} \quad (20)$$

with

$$\mathbf{K}_E = \mathbf{H}_g^T \otimes \mathbf{G} + \mathbf{H}_\theta^T \otimes \mathbf{F} \quad (21)$$

From the force-deformation equation $\delta \mathbf{f}_e = \mathbf{K} \delta \mathbf{t}$ of the end-effector, the Cartesian stiffness matrix \mathbf{K} of the robot is calculated as,

$$\mathbf{K} = \left(\mathbf{J}_\theta (\mathbf{K}_\theta - \mathbf{K}_E)^{-1} \mathbf{J}_\theta^T \right)^{-1} \quad (22)$$

3.2 Error Compensation Procedure

The motions of the industrial robots are usually generated according to the inverse kinematics, from which the input signals of the actuators $\boldsymbol{\theta}$ corresponding to the desired end-effector position \mathbf{p} are computed. However, with the external loads \mathbf{f}_e exerted to the end-effector, the kinematic control becomes non-applicable due to the compliance error $\delta \mathbf{t}$ of the end-effector, thus, the actual position is computed from the stiffness model

$$\mathbf{p}' = \mathbf{p} + \delta \mathbf{t} \quad \text{where} \quad \delta \mathbf{t} = \mathbf{K}^{-1} (\mathbf{f}_e + \mathbf{J}^{-T} \boldsymbol{\tau}) \quad (23)$$

here, $\mathbf{f}_e + \mathbf{J}^{-T} \boldsymbol{\tau}$ stands for the combination of the force and inertial forces. In order to make the end-effector be located in the desired position \mathbf{p} , the compliance error between \mathbf{p} and \mathbf{p}' , under the loads \mathbf{f}_e , should be compensated. Let

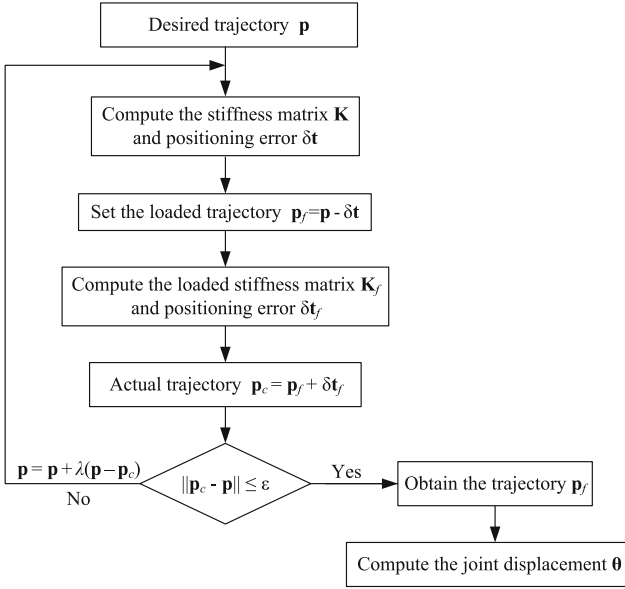


Fig. 4. Error compensation procedure for the welding robot.

suppose the modified end-effector position to be $\mathbf{p}_f = \mathbf{p} - \delta\mathbf{t}$, under the same loads \mathbf{f}_e , the actual position after compensation \mathbf{p}_c should be in the neighborhood of the desired position, namely,

$$\mathbf{p}_c = \mathbf{p}_f + \delta\mathbf{t}_f \approx \mathbf{p} \quad \text{where} \quad \delta\mathbf{t}_f = \mathbf{K}_f^{-1}(\mathbf{f}_e + \mathbf{J}_f^{-T}\boldsymbol{\tau}_f) \quad (24)$$

where \mathbf{K}_f is the stiffness matrix evaluated at the deflected position, and \mathbf{J}_f and $\boldsymbol{\tau}_f$ are the Jacobian and joint torque at the actual positions, respectively. As a consequence, the modified end-effector location \mathbf{p}_f can be calculated from the following iterative procedure,

$$\mathbf{p}'_c = \mathbf{p} + \lambda(\mathbf{p} - \mathbf{p}_c) \quad (25)$$

where the prime term corresponds to the next iteration, and $\lambda = \Delta_t / \|\mathbf{p} - \mathbf{p}_c\|$ is the scalar parameter to achieve the convergence, Δ_t being the maximum magnitude among the elements in $\mathbf{p} - \mathbf{p}_c$. This iterative method, presented in Fig. 4, will stop until $\|\mathbf{p} - \mathbf{p}_c\| \leq \epsilon$, where ϵ is an acceptable tolerance. Using this procedure to modify the reference trajectory in the robotic control, it is possible to compensate compliance errors to follow accurately the desired trajectory.

4 Case Study of Error Compensation

The previously presented stiffness modeling and error compensation procedure are illustrated with the welding robot under study, namely, the ABB IRB 4600

robot, along a trajectory as displayed in Fig. 5 together with the motion profiles of the end-effector. Based upon the FEA based evaluation, the upper arm and forearm can be treated as rigid links, compared to the actuation stiffness as listed in Table 2. Other detailed technical parameters and specifications of the robot can be found from the user manual [1], and the external wrench applied to the robot end-effector is supposed to be pure forces $\mathbf{f}_e = [200 \ -200 \ -200]^T$, which is considered to be constant. Here, the requirement on the welding accuracy is higher than 0.5 mm.

Table 2. Joint stiffness values of the welding robot (unit: $[10^6 \cdot \text{Nm/rad}]$).

$K_{act,1}$	$K_{act,2}$	$K_{act,3}$	$K_{act,4}$	$K_{act,5}$	$K_{act,6}$
0.237	3.32	2.79	0.486	0.521	0.38

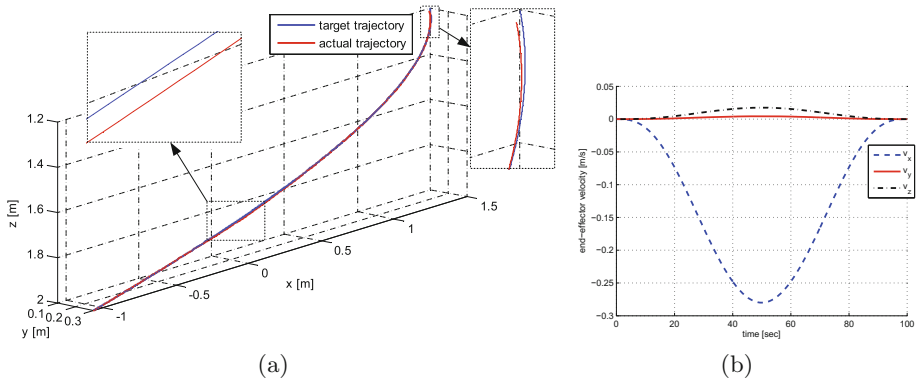
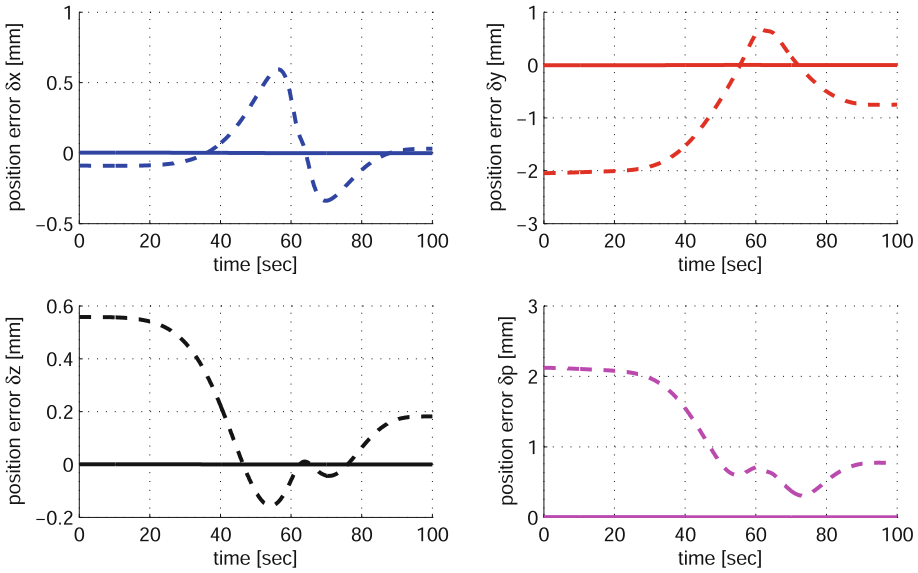
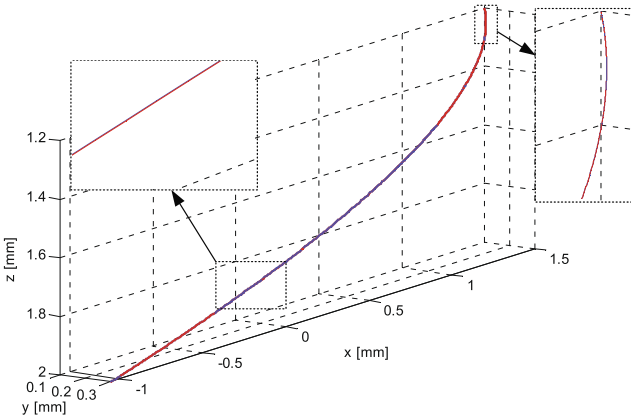


Fig. 5. The motion profiles of the welding robot: (a) desired and actual trajectories without error compensation; (b) end-effector velocities.

Figure 6 shows the comparison of the positioning errors and trajectories before and after compensation. It is seen that the maximum positioning error can be reduced to 0.01 mm when the robot tracks the modified trajectory, meaning that the positioning error after compensation can be ignored as it is much smaller than the acceptable error. Compared to the positioning error without compensation, the robot accuracy improves around 98%, which makes the actual trajectory after compensation coincident with the desired trajectory approximately, as shown in Fig. 6(b). The comparison reveals that the approach of error compensation can effectively improve the operational accuracy of the robot, also applicable to other industrial applications, such as milling.



(a)



(b)

Fig. 6. The positioning errors and trajectory after compensation: (a) positioning errors (dashed line—before compensation; solid line—after compensation); (b) comparison of target and actual trajectories.

5 Conclusions

This paper deals with the kinetostatic modeling and compliance error compensation for an industrial robot in the ship hull welding. Besides the actuation and structural stiffness, the Cartesian stiffness matrix of the robot is derived with the consideration of the arm gravity and the external loads in the welding

process as well as the inertial forces. An iterative error compensation method is introduced and is numerically illustrated along a welding trajectory. The results show that the error compensation procedure can effectively improve the operational precision to make the manipulator track the desired trajectory within acceptable positioning errors. The proposed approach implies that the manipulator accuracy can be effectively improved when the control strategy is based on the combination of the kinematic, kinetostatic and dynamic models, which is applicable to other industrial applications, such as machining.

Acknowledgement. The reported work is partly supported by the National Science and Technology Major Project (No. 2013ZX04003041-6), the Fundamental Research Funds for the Central Universities (No. DUT16RC(3)068), and the Liaoning Province STI major projects (No. 2015106007).

References

1. ABB IRB 4600 Product specification. <http://new.abb.com/products/robotics/en/industrial-robots/irb-4600>
2. Alici, G., Shirinzadeh, B.: Enhanced stiffness modeling, identification and characterization for robot manipulators. *IEEE Trans. Robot.* **21**(4), 554–564 (2005)
3. Bolmsjö, G., Olsson, M., Cederberg, P.: Robotic arc welding-trends and developments for higher autonomy. *Ind. Robot* **29**(2), 98–104 (2002)
4. Chen, S.F., Kao, I.: Conservative congruence transformation for joint and cartesian stiffness matrices of robotic hands and fingers. *Int. J. Robot. Res.* **19**, 835–847 (2000)
5. Denavit, J., Hartenberg, R.: A kinematic notation for lower-pair mechanisms based on matrices. *ASME J. Appl. Mech.* **22**, 215–221 (1955)
6. Dépincé, P., Hasco, J.Y.: Active integration of tool deflection effects in end milling. Part 2. Compensation of tool deflection. *Int. J. Mach. Tools Manuf.* **46**(9), 945–956 (2006)
7. Eastwood, S.J., Webb, P.: A gravitational deflection compensation strategy for HPKMs. *Robot. Comput.–Integr. Manuf.* **26**(6), 694–702 (2010)
8. Huang, T., Zhao, X., Whitehouse, D.J.: Stiffness estimation of a tripod-based parallel kinematic machine. *IEEE Trans. Robot. Autom.* **18**(1), 50–58 (2002)
9. Jalon, J.G.D., Bayo, E.: *Kinematic and Dynamic Simulation of Multibody Systems: The Real Time Challenge*. Springer, New York (2011)
10. Klimchik, A., Pashkevich, A., Chablat, D., Hovland, G.: Compliance error compensation technique for parallel robots composed of non-perfect serial chains. *Robot. Comput.–Integr. Manuf.* **29**(2), 385–393 (2013)
11. Kövecses, J., Angeles, J.: The stiffness matrix in elastically articulated rigid-body systems. *Multibody Syst. Dyn.* **18**(2), 169–184 (2007)
12. Meggiolaro, M.A., Dubowsky, S., Mavroidis, C.: Geometric and elastic error calibration of a high accuracy patient positioning system. *Mech. Mach. Theory* **40**(4), 415–427 (2005)
13. Pashkevich, A., Klimchik, A., Chablat, D.: Enhanced stiffness modeling of manipulators with passive joints. *Mech. Mach. Theory* **46**(5), 662–679 (2011)
14. Quennouelle, C., Gosselin, C.M.: Stiffness matrix of compliant parallel mechanisms. In: Lenarčič, J., Wenger, P. (eds.) *Advances in Robot Kinematics: Analysis and Design*, pp. 331–341. Springer, Netherlands (2008). doi:[10.1007/978-1-4020-8600-7_35](https://doi.org/10.1007/978-1-4020-8600-7_35)

15. Salisbury, J.: Active stiffness control of a manipulator in cartesian coordinates. In: 19th IEEE Conference on Decision and Control Symposium on Adaptive Processes, vol. 19, pp. 95–100 (1980)
16. Siciliano, B., Khatib, O.: Springer Handbook of Robotics. Springer, Heidelberg (2016). doi:[10.1007/978-3-319-32552-1](https://doi.org/10.1007/978-3-319-32552-1)
17. Tsai, L.: Robot Analysis: The Mechanics of Serial and Parallel Manipulators. Wiley, Hoboken (1999)
18. Wittbrodt, E., Adamiec-Wójcik, I., Wojciech, S.: Dynamics of Flexible Multibody Systems. Springer, Heidelberg (2006). doi:[10.1007/978-3-540-32352-5](https://doi.org/10.1007/978-3-540-32352-5)
19. Wu, G., Bai, S., Kepler, J.: Mobile platform center shift in spherical parallel manipulators with flexible limbs. *Mech. Mach. Theory* **75**, 12–26 (2014)
20. Wu, G., Guo, S., Bai, S.: Compliance modeling and error compensation of a 3-parallelogram lightweight robotic arm. In: Bai, S., Ceccarelli, M. (eds.) *Recent Advances in Mechanism Design for Robotics*. MMS, vol. 33, pp. 325–336. Springer, Cham (2015). doi:[10.1007/978-3-319-18126-4_31](https://doi.org/10.1007/978-3-319-18126-4_31)
21. Zhuang, H.: Self-calibration of parallel mechanisms with a case study on Stewart platforms. *IEEE Trans. Robot. Autom.* **13**(3), 387–397 (1997)